Applied Catalysis B: Environmental 204 (2017) 497–504

Contents lists available at ScienceDirect

Applied Catalysis B: Environmental

journal homepage: www.elsevier.com/locate/apcatb

Research Paper

Visible-light-driven catalytic activity enhancement of Pd in AuPd nanoparticles for hydrogen evolution from formic acid at room temperature

Penglong Liu, Xiaojun Gu*, Hao Zhang, Jia Cheng, Jin Song, Haiquan Su*

Inner Mongolia Key Laboratory of Coal Chemistry, School of Chemistry and Chemical Engineering, Inner Mongolia University, Hohhot, 010021, Inner Mongolia, China

ARTICLE INFO

Article history:
Received 8 September 2016
Received in revised form
16 November 2016
Accepted 28 November 2016
Available online 28 November 2016

Keywords:
Hydrogen evolution
Formic acid
Bimetallic nanoparticles
Photocatalysis
Palladium

ABSTRACT

A series of bimetallic AuPd nanoparticles (NPs) supported by graphene oxide (GO) were synthesized using a facile impregnation-reduction method, which were used as catalysts for the hydrogen evolution reaction (HER) from formic acid (HCOOH) under visible light irradiation at 298 K. The results showed that the bimetallic catalysts strongly absorbed visible light, and in comparison with the activities of all the catalsyts with various molar ratios of Au/Pd in the dark, their activities were remarkably enhanced under visible light irradiation. Especially, Au_1Pd_2/GO exhibited the highest activity featuring initial turnover frequency (TOF) value of 954.2 h^{-1} at 298 K, which was among the highest values for the reported heterogeneous catalysts. The enhanced photocatalytic activities of bimetallic catalysts could be mainly attributed to the efficient electron transfer from inactive Au species with localized surface plasmon resonance (LSPR) effect to active Pd sites. Support GO in the catalysts could be regarded as the electron collector and transporter and then also contributed to the enhanced catalytic activity. Furthermore, the catalytic activity of Au_1Pd_2/GO strongly depended on the intensity and wavelength of incident light, indicating that the visible light irradiation indeed played a key role in the enhanced catalytic activity.

1. Introduction

Among various energy, hydrogen featuring high heat value and clean characteristics, has attracted considerable attention as an ideal alternative to petrochemical energy [1–4]. Currently, searching for effective hydrogen storage materials and methods for hydrogen generation in safe and efficient ways remains one of the most difficult challenges toward a fuel-cell-based hydrogen economy [5–13]. Formic acid (HCOOH, FA) is a promising hydrogen carrier since it has high energy density and can be obtained by biomass processing and artificial photocatalytic CO_2 reduction [14–25]. For hydrogen-based energy application, it is desirable to develop high-performance heterogeneous metal catalysts, among which palladium (Pd) is testified as the most active component for FA dehydrogenation ($HCOOH \rightarrow CO_2 + H_2$) [26–39]. Since the dynamics of FA dehydrogenation is dependent on the temperature during the catalytic reaction [40–42], one effective and popular approach to enhancing the performance of FA dehydrogenation is to heat the catalytic system using electric energy. However, the electric energy is mainly made from fossil resources, which are non-renewable and also easily pollute the environment. Therefore, the development of new approaches to enhance the performance of FA dehydrogenation over Pd-based catalysts, which uses renewable clean energy as catalytic driving force, is highly desirable.

The utilization of sunlight, the abundant and green energy source, can shift the thermodynamic emphasis of catalytic reactions with high performance from depending on heating to favoring at ambient temperatures, which can not only reduce conventional energy consumption but also avoid unwanted byproducts formed at higher temperatures [43–51]. For the decomposition of FA, at higher temperatures the dehydration reaction easily generated CO ($HCOOH \rightarrow CO + H_2O$), which is a fatal poison to the catalysts of fuel cells. If the catalytic reaction is performed under visible light irradiation at ambient temperatures, the dehydration of FA would be avoided. As is known, gold (Au) nanoparticles (NPs) exhibit visible-light absorption due to the localized surface plasmon resonance (LSPR), resulting in that Au NPs can efficiently harvest light energy for chemical processes [52–57]. More importantly, due to the LSPR effect, the conduction electrons of Au NPs can gain the

* Corresponding authors.
E-mail addresses: xiaojun.gu@yahoo.com (X. Gu), haiquansu@yahoo.com, haiquansu@sina.com (H. Su).

http://dx.doi.org/10.1016/j.apcatb.2016.11.059
0926-3373/

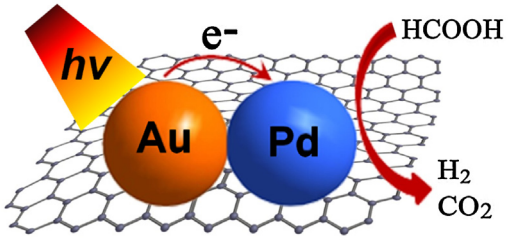

Fig. 1. Schematic illustration for AuPd/GO on FA dehydrogenation under visible light irradiation.

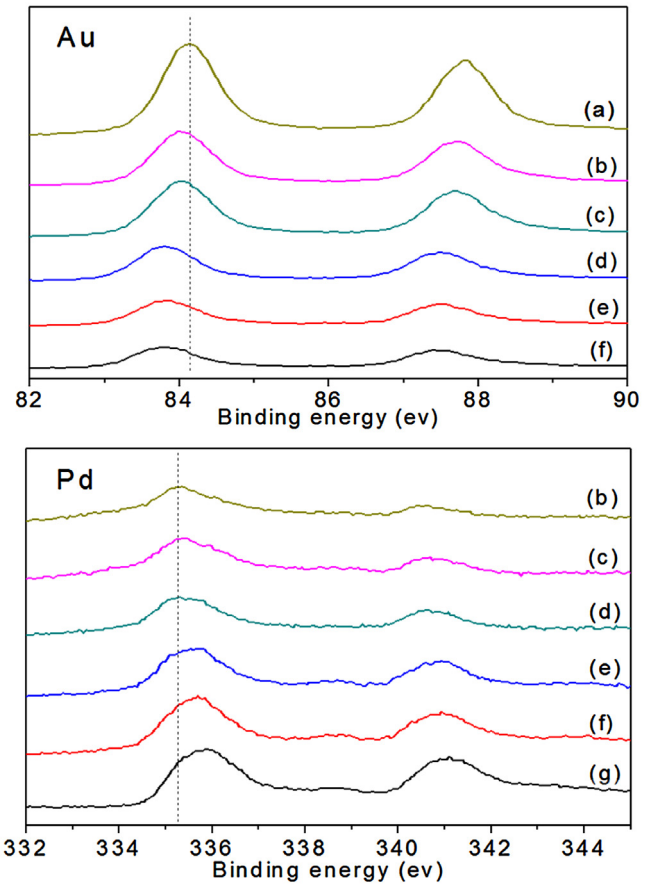

Fig. 2. XPS patterns of Au 4f and Pd 3d regions of (a) Au/GO, (b) Au_3Pd_1/GO, (c) Au_2Pd_1/GO, (d) Au_1Pd_1/GO, (e) Au_1Pd_2/GO, (f) Au_1Pd_3/GO and (g) Pd/GO.

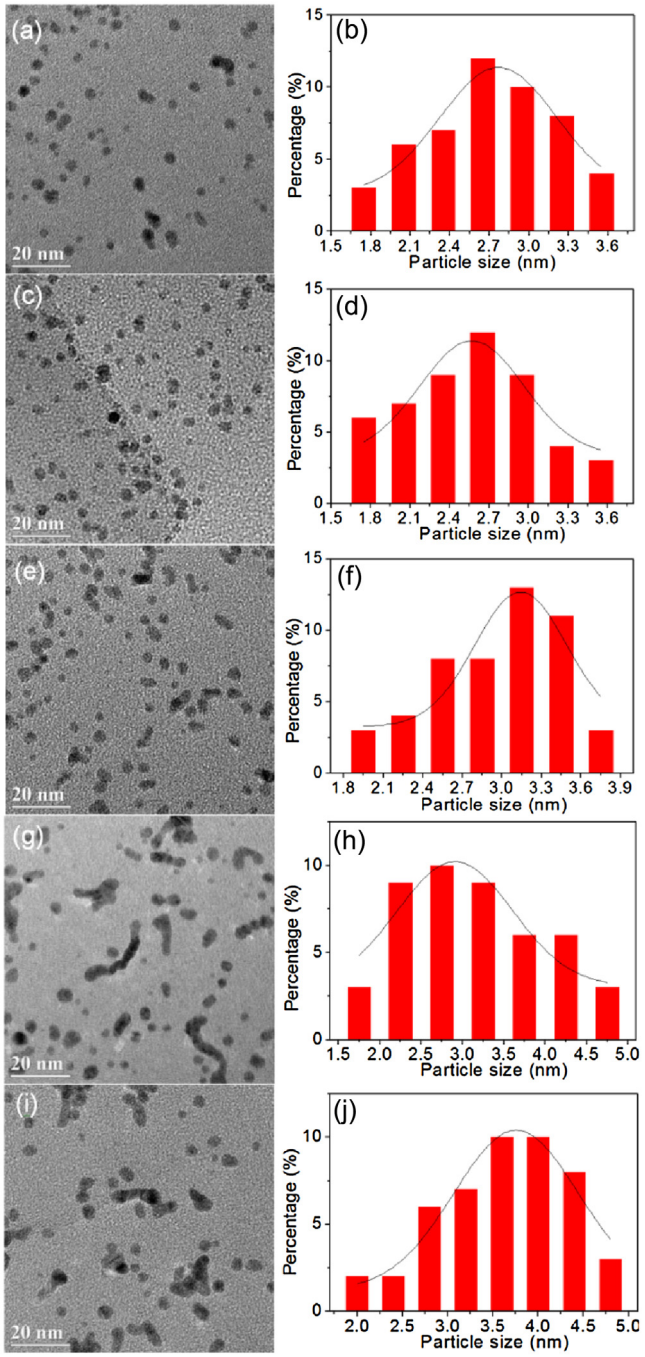

Fig. 3. TEM images of the as-synthesized catalysts and the corresponding size distributions of AuPd NPs: (a, b) Au_1Pd_3/GO; (c, d) Au_1Pd_2/GO; (e, f) Au_1Pd_1/GO; (g, h) Au_2Pd_1/GO; (I, j) Au_3Pd_1/GO.

irradiation energy, leading to high energy electrons at their surface [58–60]. From the above mentioned aspects, it can be envisioned that under visible light irradiation the energetic electrons of inactive Au species would be transferred to active Pd sites in bimetallic alloy AuPd NPs, leading to the electron density enrichment of active Pd sites and the resulting superior catalytic performance on FA dehydrogenation at room temperature (298 K).

Herein, we reported a series of bimetallic AuPd NPs supported by graphene oxide (GO), which were used as catalysts for FA dehydrogenation. As expected that the as-synthesized catalysts exhibited remarkably enhanced activities and 100% of H_2 selectivity under visible light irradiation at 298 K. Moreover, the catalytic mechanism and the influence of visible light wavelength and intensity on the catalytic performance were also discussed.

2. Experimental

2.1. Chemicals

All chemicals were commercial and were employed with no further purification. FA (HCOOH, Sigma-Aldrich, 99%), sodium formate (HCOONa, SF, Sigma-Aldrich, 99%), palladium chloride ($PdCl_2$, Sinopharm Chemical Reagent Co., Ltd, 99%), sodium chloride (NaCl, Sinopharm Chemical Reagent Co., Ltd, 99%), tetrachloroauric acid ($HAuCl_4{\cdot}4H_2O$, Sinopharm Chemical Reagent Co., Ltd, 99%), sodium borohydride ($NaBH_4$, J&K Chemical, 99%), lysine (J&K Chemical, 99%), graphite (C, ACROSS, 99%), sulfuric acid (H_2SO_4,

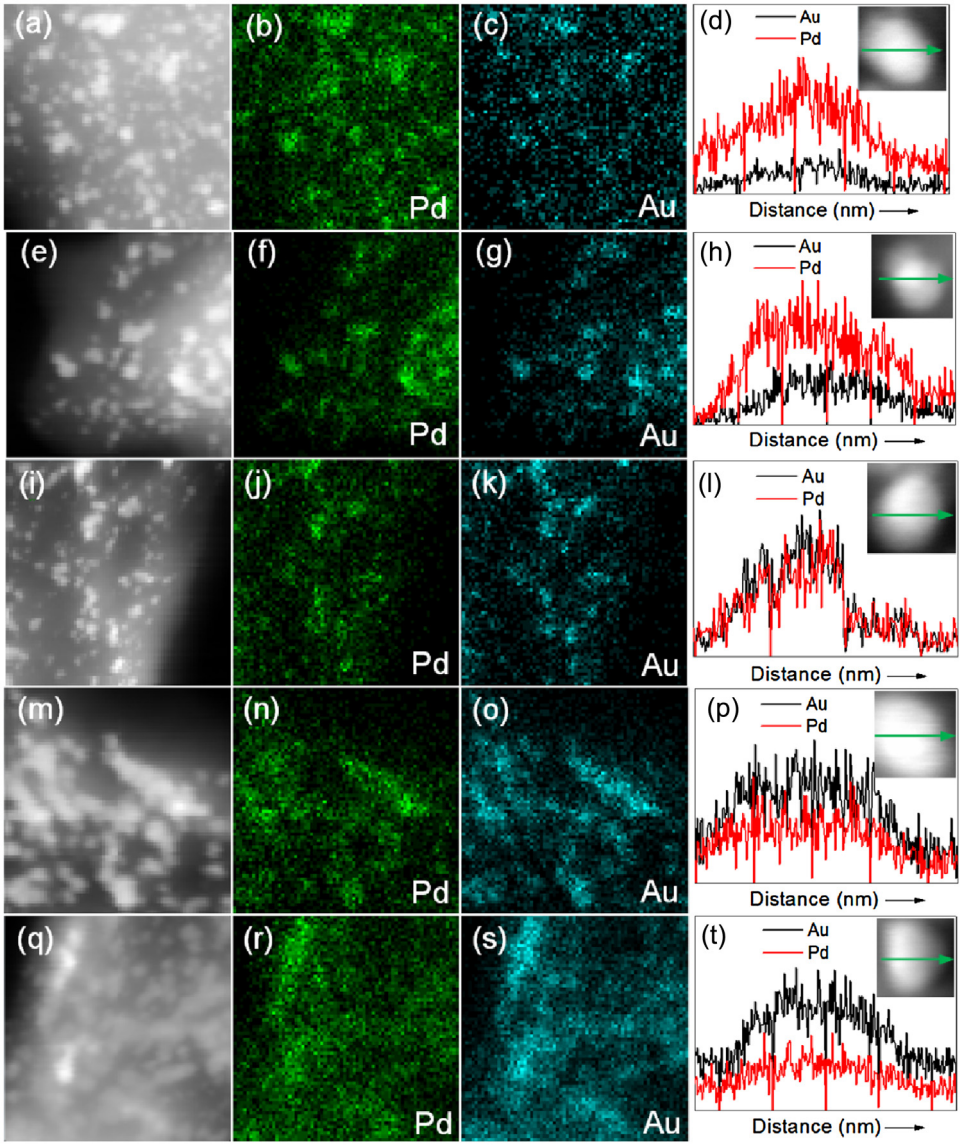

Fig. 4. HAADF-STEM images of the catalysts and the corresponding elemental mapping images for Au and Pd as well as the HAADF-STEM line-scanning analysis for Au and Pd along the green arrow given in the HAADF-STEM image (inset): (a, b, c, d) Au_1Pd_3/GO; (e, f, g, h) Au_1Pd_2/GO; (i, j, k, l) Au_1Pd_1/GO; (m, n, o, p) Au_2Pd_1/GO; (q, r, s, t) Au_3Pd_1/GO. (For interpretation of the references to colour in this figure legend, the reader is referred to the web version of this article.)

Tianjin Yaohua Chemical Reagent Co., Ltd, 95–98%), potassium permanganate (KMnO, 99%), graphite (C, ACROSS, 99%), sulfuric acid (H_2SO_4, Tianjin Yaohua Chemical Reagent Co., Ltd, 95–98%), potassium permanganate ($KMnO_4$, Beijing Chemical Reagent Co., Ltd, 99.5%), sodium nitrite (Sinopharm Chemical Reagent Co., Ltd, 99%), Al_2O_3 (Alfa Aesar Chemical Co. Ltd, 99.7%), poly(ethylene glycol)-block-poly(propylene glycol)-block-poly(ethylene glycol) (P123, Sigma-Aldrich, $M_n = 5800$), hydrochloric acid (HCl, Tianjin Fengchuan Chemical Reagent Technologies Co., Ltd, 36%) and tetraethyl orthosilicate (TEOS, Sinopharm Chemical Reagent Co., Ltd, >99%) were used. Deionized H_2O was used in all experiments.

2.2. Synthesis and catalytic study

The aqueous solution of Na_2PdCl_4 was prepared by dissolving $PdCl_2$ (1.0 g) and NaCl (0.65 g) into 50 mL of water with magnetic stirring for 10 h at room temperature. GO was prepared via modified Hummers method [61]. All the catalysts were synthesized using an impregnation-reduction process. For the synthesis of Au_1Pd_2/GO, 10 mL of aqueous solution containing $HAuCl_4{\cdot}4H_2O$ (0.13 mmol) and Na_2PdCl_4 (0.27 mmol) was mixed with 10 mL of aqueous solution of GO (5.0 mg/mL) in a flask and kept under vigorous stirring for 1 h. After that, 6 mL of aqueous solution containing lysine (3.0 mmol) was added into the above mixture and kept under vigorous stirring for 1 h. Then, 8 mL of aqueous solution containing $NaBH_4$ (1.2 mmol) was added into the flask. After stirring for 3 h, the catalyst was obtained by centrifugation, washing and drying.

Through tuning the molar ratios of Au/Pd and different supports, other nine catalysts were synthesized. The preparation process of six catalysts Au_1Pd_3/GO, Au_1Pd_1/GO, Au_2Pd_1/GO, Au_3Pd_1/GO, Au/GO and Pd/GO and three catalysts Au_1Pd_2/Al_2O_3, Au_1Pd_2/SBA-15 and Au_1Pd_2 without support was similar to that of Au_1Pd_2/GO except for the different molar ratios of Au/Pd and different supports, respectively.

For the catalytic study, the as-prepared catalyst was kept in a two-necked round-bottom flask with light window. One neck was connected to a gas burette, and the other was connected to a pressure-equalization funnel to introduce the aqueous solution containing FA. The catalytic reaction began once 4.0 mL of aqueous solution of FA (1.0 M) and SF (1.0 M) was injected into the flask

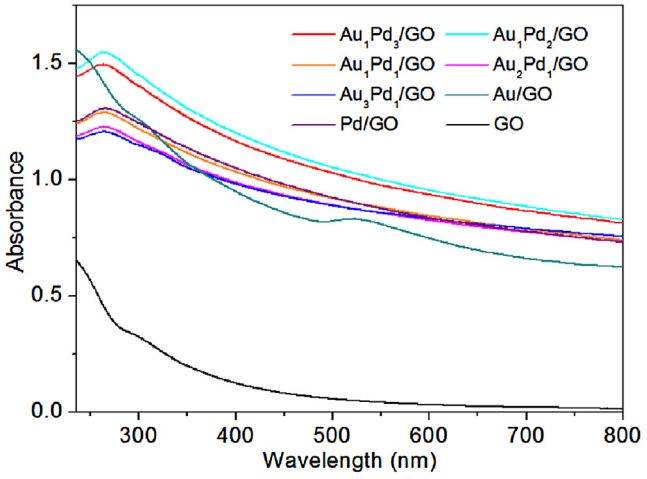

Fig. 5. UV–vis spectra of GO, monometallic and bimetallic catalysts.

under visible light irradiation using various quartz filters or in the dark. The evolution of gas was monitored using the gas burette. The temperature during the photocatalytic reactions was kept at 298 K. The molar ratio for metal/FA was kept a constant of 0.01:1 in all the catalytic processes.

2.3. Calculation methods

Since the sizes of AuPd NPs were less than 5.0 nm and they were well dispersed on the supports, all the Au and Pd species in AuPd NPs could be considered as catalytically active sites in the catalytic reaction. Therefore, the TOF value was calculated from the equation as follow:

$$TOF = \frac{P_{atm}V_{gas}/RT}{2n_{metal}t}$$

In the equation, P_{atm} (88.8 kPa) is the atmospheric pressure in Hohhot of Inner Mongolia, V_{gas} is the volume of generated H_2 and CO_2, R is the universal gas constant (8.314 m^3 Pa mol^{-1} K^{-1}), T is 298 K, n_{metal} is the total mole amounts of metal atoms in the catalyst, and t is the reaction time.

2.4. Characterization

Powder X-ray diffraction (PXRD) measurements were performed on a Panalytical X-Pert X-ray diffractmeter. The X-ray photoelectron spectra (XPS) were acquired with an ESCALAB250 (Thermo VG Corp.). The transmission electron microscope (TEM, JEM-2010) equipped with an energy dispersive X-ray spectrometer (EDS) for elemental analysis was applied for the morphologies and composition of the as-synthesized samples. Detailed analyses for CO_2, H_2 and CO were performed on Shimadzu GC-2014 with thermal conductivity detector (TCD) and hydrogen flame ionization detector (FID)-Methanator (detection limit: 10 ppm). The UV–vis spectra were conducted on a Shimadzu UV-3600. Inductively coupled plasma-atomic emission spectroscopy (ICP-AES) measurement was performed on a Thermo Jarrell Ash (TJA) Atomscan Advantage instrument.

3. Results and discussion

Among various catalyst supports, GO with 2D planar π-conjugation structure was selected as the electron collector and transporter to transfer the electron from Au to active Pd sites, leading to the enhanced performance of AuPd catalysts on FA dehydrogenation. Recently, we have reported that the catalytic performance of metal NPs can be tuned through the selection of amino acids as structuring agents [13]. Therefore, in order to remarkably enhance the performance on FA dehydrogenation, GO and lysine were selected as support and structuring agent, respectively, to synthesize supported AuPd catalysts. On the basis of the above synthesis considerations including LSPR effect of Au, the as-synthesized AuPd/GO catalysts would exhibit high catalytic performance on FA dehydrogenation under visible light irradiation at 298 K (Fig. 1).

The PXRD patterns of every AuPd catalyst showed a broad peak between the characteristic peaks for Au (111) and Pd (111) (Fig. S1), indicating the formation of the AuPd alloy. The gradual shift of (111) reflection towards higher angles with a decrease of the molar ratio of Au/Pd also suggested the formation of AuPd alloy, which ensured the efficient electron transfer from Au to Pd species and thus the resulting enhanced catalytic performance of AuPd catalysts. It should be noted that there was the slight non-symmetry of (111) reflection of AuPd NPs due to their small size-induced broadening of adjacent diffraction peaks [62,63]. The XPS investigation showed that the binding energies of Au 4f and Pd 3d in bimetallic AuPd/GO catalysts with various ratios of Au/Pd shifted to lower values compared to those in monometallic Au/GO and Pd/GO (Fig. 2). These shifts demonstrated that there were strong interactions between GO and metal NPs and then some electrons were transferred from GO to AuPd NPs in the catalysts [50,60]. The strong interactions also ensured that GO could be used as the electron transporter to transfer the electron from Au with LSPR effect to active Pd sites under visible light irradiation. Moreover, the formation of AuPd alloy NPs could also result in the electron transfer from Au to Pd to equilibrate the Fermi level because of the different work functions of Pd (5.67 eV) and Au (5.54 eV) [30]. For the sake of further exploring the effect of graphene on the electronic state of Pd species in AuPd catalysts, one catalyst Au_1Pd_2 without support was synthesized and the XPS comparison of Au_1Pd_2/GO and Au_1Pd_2 was studied. The results exhibited that binding energies of Pd 3d in Au_1Pd_2/GO shifted to lower values compared to those in Au_1Pd_2 (Fig. S2), indicating the GO could effectively transfer the electron from Au to active Pd sites and then induced the enhanced electronic density of Pd species in the bimetallic AuPd NPs. The TEM images showed that the average sizes of Au_1Pd_3, Au_1Pd_2, Au_1Pd_1, Au_2Pd_1 and Au_3Pd_1 NPs in AuPd/GO were 2.8 ± 0.5, 2.7 ± 0.5, 3.2 ± 0.5, 2.8 ± 0.5 and 3.9 ± 0.5 nm, respectively (Fig. 3). Among these catalysts, Au_1Pd_3, Au_1Pd_2 and Au_1Pd_1 NPs had the high dispersion on the surface of GO, while Au_2Pd_1 and Au_3Pd_1 NPs had obvious aggregation. These different structures and morphologies of AuPd NPs in these catalysts might result in the different catalytic activities. The elemental mapping corresponded to a high-angel annular dark-field scanning TEM (HAADF-STEM) image showed that the elements of Au and Pd were homogeneously distributed in the randomly selected area (Fig. 4), indicating the formation of homogeneous AuPd NPs dispersed on GO supports in the five catalysts Au_1Pd_3/GO, Au_1Pd_2/GO, Au_1Pd_1/GO, Au_2Pd_1/GO and Au_3Pd_1/GO. The formation of AuPd alloy structure was further confirmed by the HAADF-STEM-line analysis. In detail, when the distribution of Au and Pd in the randomly chosen particle was assessed using the STEM-EDS mode, it was seen that the molar ratios of Au/Pd were approximately same to the theoretical values in the catalysts and both Au and Pd atoms were homogeneously observed in the cross-section (Fig. 4d, h, l, p and t). Especially, the overlapping of Au and Pd signals was found in Au_1Pd_1/GO with the equal molar ratio of Au/Pd. The above results gave the evidence for the formation of AuPd alloy structures in the five catalysts. In addition, the EDS results showed that Au and Pd were incorporated in the catalysts (Fig. S3-S7). The actual molar ratios Au/Pd in the five catalysts Au_1Pd_3/GO, Au_1Pd_2/GO, Au_1Pd_1/GO, Au_2Pd_1/GO and Au_3Pd_1/GO were 1:3.13,

1:2.04, 1.02:1, 2.11:1 and 3.15:1 calculated by the ICP-AES results, respectively (Table S1).

From the UV–vis spectra (Fig. 5), it could be found that the spectra of the AuPd samples were clearly different from the spectrum of the pure Au sample. GO exhibited a weak visible light absorption, and therefore, the GO support itself did not contribute to the photocatalytic activity [64]. In contrast, all the Au, Pd, and AuPd alloy NPs on the GO supports displayed high levels of absorption in the UV and visible range, indicating that solar energy was strongly coupled to the metal NPs. Since the sizes of metal NPs affect the LSPR intensity, the characteristic absorption peak at around 520 nm in the spectrum of the pure Au NPs sample with small sizes was broadened [65]. In addition, the presence of the GO support and its interaction with Au in the AuPd NPs might broaden this peak.

In order to explore the catalytic behaviors of AuPd/GO, the catalytic hydrogen evolution from FA was tested under visible light irradiation and in the dark. It should be noted that in order to eliminate the thermal influence on catalytic performance, the reaction temperature was kept under visible light irradiation at 298 K. Compared to the catalytic performance in the dark, all the catalytic performance, especially activity, on hydrogen evolution from FA over all the AuPd/GO catalysts under visible light irradiation was remarkably enhanced (Fig. 6). Among all the catalysts, Au_1Pd_2/GO exhibited the highest activity featuring the initial TOF value of 954.2 h^{-1}, which was among the highest values for the reported heterogeneous catalysts for FA dehydrogenation at 298 K [15–36]. The GC analysis confirmed equal molar amount of CO_2 and H_2 in the gas mixture generated by FA decomposition over Au_1Pd_2/GO (Fig. S9a), indicating the complete FA dehydrogenation under visible light irradiation. Moreover, there was no CO detected in the mixture of H_2 and CO_2, which was crucial for fuel cell applications (Fig. S9b). It should be noted that no gas was detected from the hydrolysis of SF under visible light irradiation at 298 K (Fig. S10), which again verified that the bimetallic catalyst promoted complete decomposition of FA into H_2 and CO_2.

From Fig. 6, it could be also found that there were different enhancement extents of activities of catalysts with different molar ratios of Au/Pd. The highest and the lowest enhancement extents were about 145% and 92% for Au_1Pd_1/GO and Pd/GO, which implied that the catalytic activity under visible light irradiation was dominated by Pd though the alloying of Au and Pd in the bimetallic catalysts. This provided a design criteria for selecting other metals to alloy with Au to catalyze specific reactions with light driven processes. Moreover, the dependence on the molar ratios of Au/Pd in the alloy NPs for FA dehydrogenation in the dark was similar to that observed for the light-enhanced reaction but with much lower activities. These results showed while light illumination and alloy composition both impacted on catalytic performance of the alloy NPs, the visible light irradiation had a more pronounced effect than the molar ratios of Au/Pd. One possible explanation for these observations was that the charge heterogeneity at the alloy NPs' surface resulted in the improved catalytic activity of the alloy structure [66]. At the Au/Pd ratio of 1:2, the surface charge heterogeneity was optimal for the catalysis both in the presence and absence of light. The increased charge heterogeneity implied that the interactions between the alloy NPs and reactant molecule FA were enhanced. When the alloy NPs were irradiated with visible light, the conduction electrons were elevated into excited states through absorption of light energy, leading to the catalytic capability increase of alloy NPs.

In order to further confirm the role of Au in enhancing the catalytic performance of Pd catalysts, the monometallic Au and Pd catalysts Au/GO and Pd/GO were synthesized and their catalytic performance was studied. The results showed that compared to Pd/GO with low activity and H_2 selectivity and Au/GO without activity, Au_1Pd_2/GO exhibited high activity and 100% of H_2 selectivity not only under visible light irradiation but also in the dark (Fig. 7). These differences illustrated that in the two influencing factors, namely, visible light illumination and alloying effect, the visible light illumination was the key in enhancing the catalytic activity on FA dehydrogenation using the LSPR effect of Au. In addition, in order to confirm the role of GO in enhancing the catalytic performance of AuPd catalysts, Au_1Pd_2 catalyst without support was synthesized and the catalytic performance of Au_1Pd_2, Au_1Pd_2/GO and GO were compared under visible light irradiation and in the dark. The results exhibited that compared to Au_1Pd_2/GO

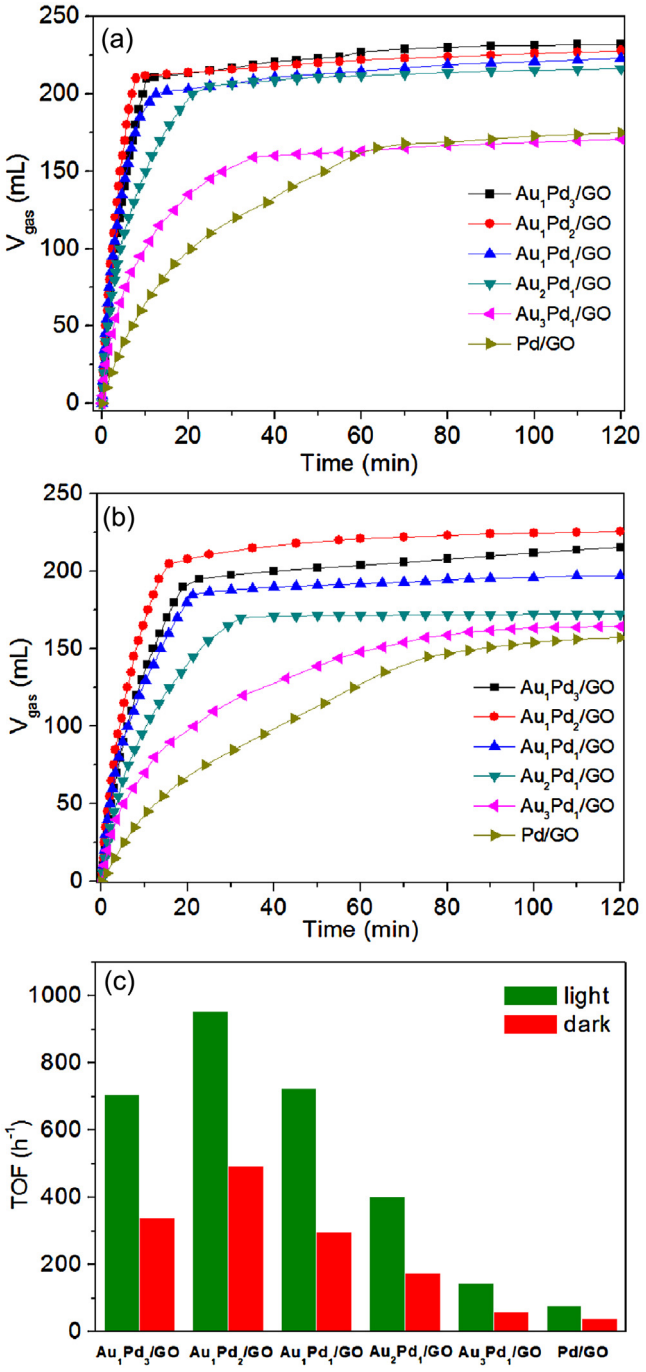

Fig. 6. Plots of time versus volume of generated gas (CO_2 and H_2) from FA-SF aqueous solution over AuPd/GO with different molar ratios of Au/Pd (a) under visible light irradiation at 298 K and (b) in the dark at 298 K as well as (c) the TOF values of the above six catalysts under visible light irradiation at 298 K and in the dark at 298 K.

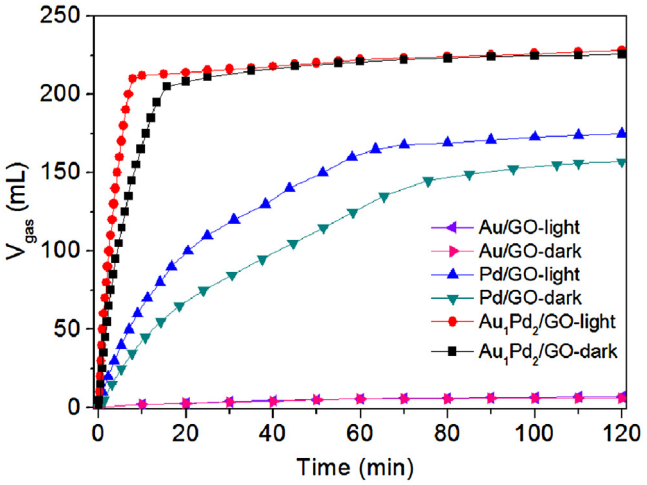

Fig. 7. Plots of time versus volume of generated gas (CO_2 and H_2) from FA-SF aqueous solution over Au/GO, Pd/GO and Au_1Pd_2/GO under visible light irradiation at 298 K and in the dark at 298 K.

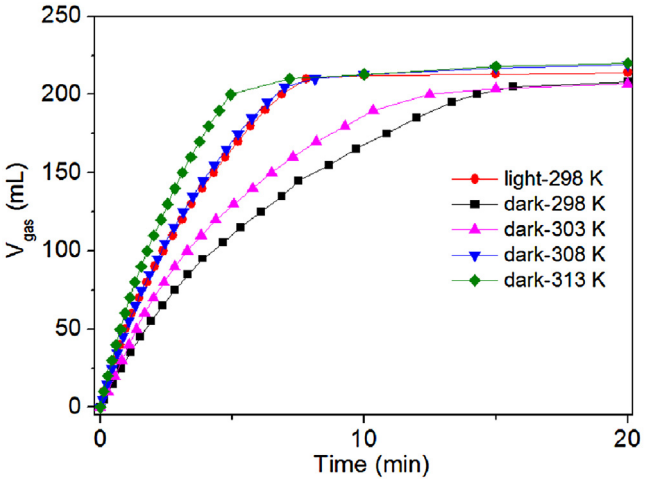

Fig. 8. Plots of time versus volume of generated gas (CO_2 and H_2) from FA-SF aqueous solution over Au_1Pd_2/GO under visible light irradiation at 298 K and in the dark at different temperatures.

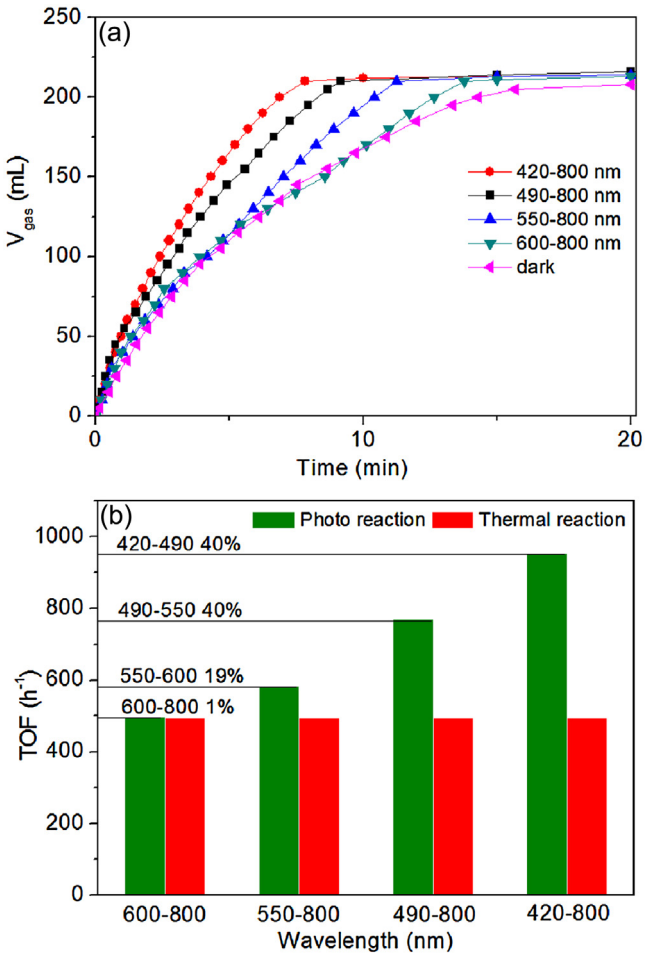

Fig. 9. (a) Plots of time versus volume of generated gas (CO_2 and H_2) from FA-SF aqueous solution over Au_1Pd_2/GO under different wavelength ranges at 298 K and (b) the corresponding dependence of the catalytic activity of Au_1Pd_2/GO on the wavelength of the light irradiation.

with high catalytic performance, Au_1Pd_2 and GO almost had not activities (Fig. S11), indicating that conducting GO indeed promoted the FA dehydrogenation of AuPd NPs. In many cases, the sizes of active metal NPs in the heterogeneous catalysts strongly affect their activities and selectivity of target product [67,68]. Herein, the AuPd NPs aggregated seriously in the support-free Au_1Pd_2 catalyst (Fig. S12), which hindered the efficient electron transfer between Au and Pd species in the AuPd NPs. As a result, its catalytic performance dramatically decreased and only 14 mL of gas (H_2 and CO_2) generated in the decomposition of FA at 298 K. Furthermore, the TEM image of Au_1Pd_2/GO after catalysis exhibited that there was no significant aggregation of AuPd NPs (Fig. S13), indicating that GO have strong ability for immobilizing AuPd NPs.

In general, increasing the temperature in the dark always can lead to the enhanced dehydrogenation rate of FA [40–42]. So in order to estimate the amount of saving energy using photocatalytic way, the catalytic FA dehydrogenation performance of Au_1Pd_2/GO in the dark at different temperatures was tested and was compared with the similar process under the visible light irradiation at 298 K (Fig. 8). Obviously, the catalytic activity under light irradiation at 298 K was approximately equal to that in the dark at 308 K, indicating that the electrons in Au excited by visible light effectively promoted the dehydrogenation rate of FA at 298 K. In order to confirm the role of SF in the present catalytic process, we have explored the effect of different molar ratios of FA/SF on hydrogen generation from FA using Au_1Pd_2/GO as catalyst. The results showed that the molar ratios of FA/SF had an obvious effect on the catalytic performance of Au_1Pd_2/GO (Fig. S14). In detail, the activity of Au_1Pd_2/GO increased with increasing the concentration of SF in the solution of FA and SF until the molar ratio of FA/SF reached 1:1, after which further increase in the concentration of SF had only a slight effect on the hydrogen generation. Moreover, Au_1Pd_2/GO had low activity and H_2 selectivity in the pure FA solution. From the above results, it could be seen that SF played an important role in enhancing the activities and H_2 selectivity of GO-supported AuPd catalysts for hydrogen generation from FA at 298 K.

In order to further understand the enhancement of the catalytic performance obtained through visible light irradiation of the AuPd NPs, the dependence of light's wavelength and intensity on the catalytic FA dehydrogenation over Au_1Pd_2/GO was investigated at 298 K. It should be noted that the single-wavelength light intensity in the range of 420 – 800 nm had no big difference in the spectrum of the light source (Fig. S15). Regarding the study of wavelength ranges, a series of optical low-pass filters were used to block light below specific cutoff wavelengths. As shown in Fig. 9, the irradiation of the light with wavelengths ranging from 420 to 800 nm gave an activity with TOF value of 954.2 h^{-1}. When the wavelength ranges of the irradiation were

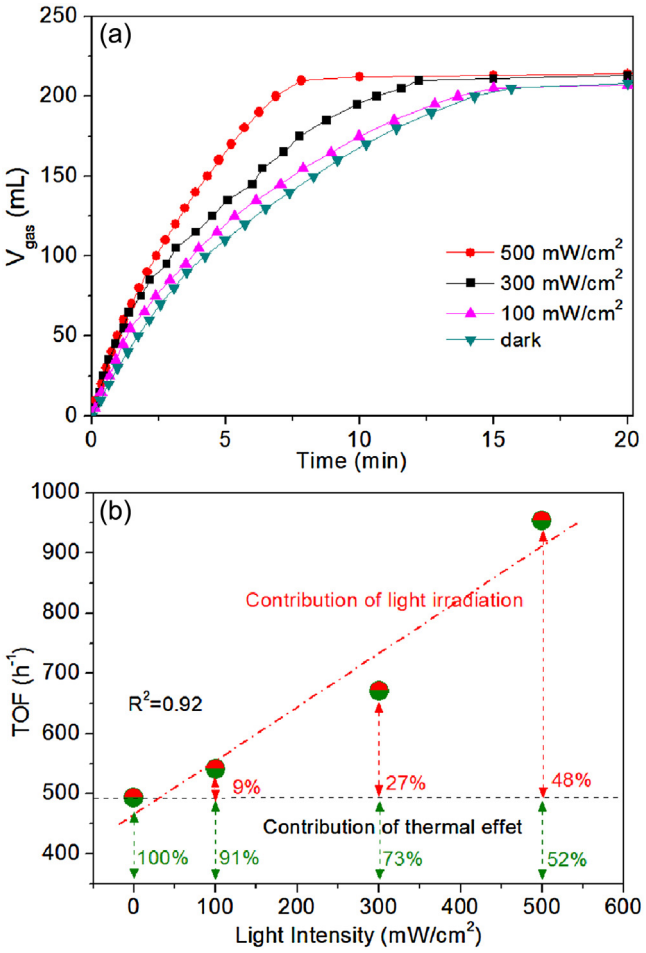

Fig. 10. (a) Plots of time versus volume of generated gas (CO_2 and H_2) from FA-SF aqueous solution over Au_1Pd_2/GO under different intensities of the light irradiation at 298 K and (b) the corresponding dependence of the catalytic activity of Au_1Pd_2/GO on the intensity of the light irradiation.

490 – 800, 550 – 800 and 600 – 800 nm, the TOF values decreased to 769.5, 584.2 and 496.4 h^{-1}, respectively. Since the TOF value in the dark was 493.6 h^{-1}, the light in the 600 – 800 nm wavelength range contributed 2.8 (496.4 – 493.6) h^{-1}, accounting for 1% (496.4 – 493.6)/(954.2 – 493.6) of the light-induced activity. Similarly, the irradiation in the wavelength ranges of 420 – 490, 490 – 550 and 550 – 600 nm contributed 184.7 (954.2 – 769.5), 185.3 (769.5 – 584.2) and 87.8 (584.2 – 496.4) h^{-1}, respectively, which accounted for about 40, 40 and 19% of the light-induced activity, respectively. From these results, it could be seen that the highest activity in visible light range was observed in 420 – 550 nm. Regarding the study of light intensity, the wavelength range of the irradiation was fixed in 420 – 800 nm. As shown in Fig. 10, increasing the light intensity resulted in an almost linear increase in the FA dehydrogenation rates. The TOF of Au_1Pd_2/GO in the dark was 493.6 h^{-1}, and the TOF was 540.8 h^{-1} under the irradiation of the light with light intensity of 100 mW/cm^2. So we could get that the contribution of light irradiation in the catalytic process was about 9% ((540.8 – 493.6)/540.8). Similarly, the contribution of light irradiation of 300 and 500 mW/cm^2 was about 27 and 48%, respectively.

There are different interactions between different metals with different supports [69–71]. So other supports Al_2O_3 and SBA-15 were selected to synthesize AuPd NPs. The TEM investigation showed that the sizes of AuPd NPs in Au_1Pd_2/Al_2O_3 and Au_1Pd_2/SBA-15 were larger than those in Au_1Pd_2/GO (Figs. S16 and S17). The catalytic results under visible light irradiation showed that Au_1Pd_2/GO had the best catalytic performance in the three catalysts Au_1Pd_2/GO Au_1Pd_2/Al_2O_3 and Au_1Pd_2/SBA-15 (Fig. S18), which might be due to the good conductivity and huge number of nonbonding electrons in the layered structure of GO. It is worth mentioning that besides the low activities of Au_1Pd_2/Al_2O_3 and Au_1Pd_2/SBA-15, they only had the H_2 selectivity of 57 and 32%, respectively, which were lower than the value (100%) of Au_1Pd_2/GO.

4. Conclusions

In conclusion, we have designed and synthesized a series of GO-supported AuPd NPs and the catalytic results demonstrated that the intrinsic activity of Pd in the FA dehydrogenation was remarkably enhanced by visible light irradiation of AuPd alloy NPs at 298 K. The efficient electron transfer from Au with LSPR effect to active Pd sites played a key role in the enhanced catalytic FA dehydrogenation under the visible light irradiation. Moreover, regulating the wavelength and intensity of light irradiation could control the activities of bimetallic catalysts, and the charge heterogeneity at the AuPd alloy surface and the utilization of graphene as the electron collector and transporter also contributed to the enhanced catalytic performance.

Acknowledgements

This work was financially supported by the Program for New Century Excellent Talents in University of the Ministry of Education of China (grant no. NCET-13-0846), the National Natural Science Foundation of China (grant no. 21101089), the Program for Young Talents of Science and Technology in Universities of Inner Mongolia Autonomous Region (grant no. NJYT-13-A01) and the Inner Mongolia Natural Science Foundation (grant no. 2011JQ01).

Appendix A. Supplementary data

Supplementary data associated with this article can be found, in the online version, at http://dx.doi.org/10.1016/j.apcatb.2016.11.059.

References

[1] P.P. Edwards, V.L. Kuznetsov, W.I. David, N.P. Brandon, Energy Policy 36 (2008) 4356–4362.
[2] J. Graetz, Chem. Soc. Rev. 38 (2009) 73–82.
[3] C.W. Hamilton, R.T. Baker, A. Staubiz, I. Manners, Chem. Soc. Rev. 38 (2009) 279–923.
[4] H.M. Chen, C.K. Chen, R.S. Liu, L. Zhang, J. Zhang, D.P. Wilkinson, Chem. Soc. Rev. 41 (2012) 5654–5671.
[5] L. Schlapbach, A. Züttel, Nature 414 (2001) 353–358.
[6] Z. Xiong, C.K. Yong, G. Wu, P. Chen, W. Shaw, A. Karkamkar, T. Autrey, M.O. Jones, S.R. Johnson, P.P. Edwards, W.I.F. David, Nat. Mater. 7 (2008) 138–141.
[7] A. Staubitz, A.P.M. Robertson, I. Manners, Chem. Rev. 110 (2010) 4079–41241.
[8] A. Boddien, D. Mellmann, F. Gärtner, R. Jackstell, H. Junge, P.J. Dyson, G. Laurenczy, R. Ludwig, M. Beller, Science 333 (2011) 1733–1736.
[9] M. Yurderi, A. Bulut, I.E. Ertas, M. Zahmakiran, M. Kaya, Appl. Catal. B: Environ. 165 (2015) 169–175.
[10] Q. Zhu, Q. Xu, Energy Environ. Sci. 8 (2015) 478–512.
[11] K. Kang, X. Gu, L. Guo, P. Liu, X. Sheng, Y. Wu, J. Cheng, H. Su, Int. J. Hydrog. Energy 40 (2015) 12315–12324.
[12] L. Guo, X. Gu, K. Kang, Y. Wu, J. Cheng, P. Liu, T. Wang, H. Su, J. Mater. Chem. A 3 (2015) 22807–22815.
[13] J. Cheng, X. Gu, X. Sheng, P. Liu, H. Su, J. Mater. Chem. A 4 (2016) 1887–1894.
[14] F. Jin, J. Yun, G. Li, A. Kishita, K. Tohji, H. Enomoto, Green Chem. 10 (2008) 612–615.
[15] K. Tedsree, T. Li, S. Jones, C.W.A. Chan, K.M.K. Yu, P.A.J. Bagot, E.A. Marquis, G.D.W. Smith, S.C.E. Tsang, Nat. Nanotechnol. 6 (2011) 302–307.
[16] S. Zhang, Ö. Metin, D. Su, S. Sun, Angew. Chem. Int. Ed. 52 (2013) 3681–3684.
[17] W. Wang, M. Niu, Y. Hou, W. Wu, Z. Liu, Q. Liu, S. Ren, K.N. Marsh, Green Chem. 16 (2014) 2614–2618.
[18] S. Lee, H. Ju, R. Machunda, S. Uhm, J.K. Lee, H.J. Lee, J. Lee, J. Mater. Chem. A 3 (2015) 3029–3034.
[19] D. Kumar, A. Lee, T. Lee, M. Lim, D. Lim, Nano Lett. 16 (2016) 1760–1767.

[20] S. Gao, Y. Lin, X. Jiao, Y. Sun, Q. Luo, W. Zhang, D. Li, J. Yang, Y. Xie, Nature 529 (2016) 68–72.
[21] T. Arai, S. Sato, T. Morikawa, Energy Environ. Sci. 8 (2015) 1998–2002.
[22] D. Won, C. Choi, J. Chung, S. Woo, Appl. Catal. B: Environ. 158 (2014) 217–223.
[23] P. Richardson, M. Perdigoto, W. Wang, R. Lopes, Appl. Catal. B: Environ. 132 (2013) 408–415.
[24] G. Qin, Y. Zhang, X. Ke, X. Tong, Z. Sun, M. Liang, S. Xue, Appl. Catal. B: Environ. 129 (2013) 599–605.
[25] M.F. Kuehnel, D.W. Wakerley, K.L. Orchard, E. Reisner, Angew. Chem. Int. Ed. 54 (2015) 9627–9631.
[26] K. Tedsree, T. Li, S. Jones, C. Chan, K. Yu, P. Bagot, E. Marquis, G. Smith, S. Tsang, Nat. Nanotech. 6 (2011) 302–307.
[27] X. Gu, Z. Lu, H. Jiang, T. Akita, Q. Xu, J. Am. Chem. Soc. 133 (2011) 11822–118251.
[28] S. Zhang, Ö. Metin, D. Su, S. Sun, Angew. Chem. Int. Ed. 52 (2013) 3681–3684.
[29] Y.-Y. Cai, X.-H. Li, Y.-N. Zhang, X. Wei, K.-X. Wang, J.-S. Chen, Angew. Chem. Int. Ed. 52 (2013) 11822–11825.
[30] Z.-L. Wang, J.-M. Yan, Y. Ping, H.-L. Wang, W.-T. Zheng, Q. Jiang, Angew. Chem. Int. Ed. 52 (2013) 4406–4409.
[31] M. Yurderi, A. Bulut, M. Zahmakiran, M. Kaya, Appl. Catal. B: Environ. 160–161 (2014) 514–524.
[32] M. Yurderi, A. Bulut, N. Caner, M. Celebi, M. Kaya, M. Zahmakiran, Chem. Commun. 51 (2015) 11417–11420.
[33] Y. Chen, Q. Zhu, N. Tsumori, Q. Xu, J. Am. Chem. Soc. 137 (2015) 106–109.
[34] L. Yang, X. Hua, J. Su, W. Luo, S. Chen, G. Cheng, Appl. Catal. B: Environ. 168 (2015) 423–428.
[35] A. Bulut, M. Yurderi, Y. Karatas, M. Zahmakiran, H. Kivrak, M. Gulcan, M. Kaya, Appl. Catal. B: Environ. 165 (2015) 324–333.
[36] M. Hattori, D. Shimamoto, H. Ago, M. Tsuji, J. Mater. Chem. A 3 (2015) 10666–10670.
[37] N. Wang, Q. Sun, R. Bai, X. Li, G. Guo, J. Yu, J. Am Chem. Soc. 138 (2016) 7484–7487.
[38] Z.-L. Wang, J.-M. Yan, Y.-F. Zhang, Y. Ping, H.-L. Wang, Q. Jiang, Nanoscale 6 (2014) 3073–3077.
[39] Y.-L. Qin, J.-W. Wang, Y.-M. Wu, L.-M. Wang, RSC Adv. 4 (2014) 30068–30073.
[40] X. Zhou, Y. Huang, W. Xing, C. Liu, J. Liao, T. Lu, Chem. Commun. 30 (2008) 3540–3542.
[41] Q. Bi, X. Du, Y. Liu, Y. Cao, H. He, K. Fan, J. Am. Chem. Soc. 134 (2012) 8926–8933.
[42] Y. Chen, Q.-L. Zhu, T. Tsumori, Q. Xu, J. Am. Chem. Soc. 137 (2015) 106–109.
[43] A. Fujishima, K. Honda, Nature 238 (1972) 37–38.
[44] X. Chen, L. Liu, P.Y. Yu, S.S. Mao, Science 331 (2011) 746–750.
[45] S. Li, S. Liu, S. Liu, Y. Liu, Q. Tang, Z. Shi, S. Ouyan–19721.
[46] Y. Ma, X. Wang, Y. Jia, X. Chen, H. Han, C. Li, Chem. Rev. 114 (2014) 9987–10043.
[47] M. Dahl, Y. Liu, Y. Yin, Chem. Rev. 114 (2014) 9853–9889.
[48] X. Lang, X. Chen, J. Zhao, Chem. Soc. Rev. 43 (2014) 473–486.
[49] Y. Zheng, L. Lin, B. Wang, X. Wang, Angew. Chem. Int. Ed. 54 (2015) 12868–12884.
[50] Q. Xiang, B. Cheng, J. Yu, Angew. Chem. Int. Ed. 54 (2015) 11350–11366.
[51] Q. Wang, T. Hisatomi, Q. Jia, H. Tokudome, M. Zhong, C. Wang, Z. Pan, T. Takata, M. Nakabayashi, N. Shibata, Y. Li, I.D. Sharp, A. Kudo, T. Yamada, K. Domen, Nat. Mater. 15 (2016) 611–615.
[52] S. Eustis, M.A. El-Sayed, Chem. Soc. Rev. 35 (2006) 209–217.
[53] S. Linic, P. Christopher, D.B. Ingram, Nat. Mater. 10 (2011) 911–921.
[54] G.V. Naik, V.M. Shalaev, A. Boltasseva, Adv. Mater. 25 (2013) 3264–3294.
[55] F. Wang, C. Li, H. Chen, R. Jiang, L.-D. Sun, Q. Li, J. Wang, J.C. Yu, C.-H. Yan, J. Am. Chem. Soc. 135 (2013) 5588–5601.
[56] Z. Zhang, S.-W. Cao, Y. Liao, C. Xue, Appl. Catal. B: Environ. 162 (2015) 204–209.
[57] Z. Zheng, T. Tachikawa, T. Majima, J. Am. Chem. Soc. 137 (2015) 948–957.
[58] W. Hou, S.B. Cronin, Adv. Funct. Mater. 23 (2013) 1612–1619.
[59] R. Jiang, B. Li, C. Fang, J. Wang, Adv. Mater. 26 (2014) 5274–5309.
[60] Q. Xiao, E. Jaatinen, H. Zhu, Chem. Asian J. 9 (2014) 3046–3064.
[61] W.S. Hummers, R.E. Offeman, J. Am. Chem. Soc. 80 (1958), 1339–1339.
[62] C. Shen, C. Hui, T. Yang, C. Xiao, J. Tian, L. Bao, S. Chen, H. Ding, H. Gao, Chem. Mater. 20 (2008) 6939–6944.
[63] P. Fageria, S. Uppala, R. Nazir, S. Gangopadhyay, C.-H. Chang, M. Basu, S. Pande, Langmuir 32 (2016) 10054–10064.
[64] X.-N. Guo, Z.-F. Jiao, G.-Q. Jin, X.-Y. Guo, ACS Catal. 5 (2015) 3836–3840.
[65] S. Sarina, H. Zhu, E. Jaatinen, Q. Xiao, H. Liu, J. Jia, C. Chen, J. Zhao, J. Am. Chem. Soc. 135 (2013) 5793–5801.
[66] S. Sarina, S. Bai, Y. Huang, C. Chen, J. Jia, E. Jaatinen, G.A. Ayoko, Z. Bao, H. Zhu, Green Chem. 16 (2014) 331–341.
[67] B.E. Hayden, Acc. Chem. Res. 46 (2013) 1858–1866.
[68] H. Mistry, R. Reske, Z. Zeng, Z.-J. Zhao, J. Greeley, P. Strasser, B.R. Cuenya, J. Am. Chem. Soc. 136 (2014) 16473–16476.
[69] N.J. Divins, I. Angurell, C. Escudero, V. Pérez-Dieste, J. Llorca, Science 346 (2014) 620–623.
[70] M.-M. Titirici, R.J. White, N. Brun, V.L. Budarin, D.S. Su, F. del Monte, J.C. Clark, M.J. MacLachlan, Chem. Soc. Rev. 44 (2015) 250–290.
[71] J. Liu, N.P. Wichramaratne, S.Z. Qiao, M. Jaroniec, Nat. Mater. 14 (2015) 763–774.